Pediatr Blood Cancer 2012;58:598–605

A Novel Dutch Mutation in *UNC13D* Reveals an Essential Role of the C2B Domain in Munc13-4 Function

Edo D. Elstak, PhD,[1] Maroeska te Loo, MD, PhD,[2] Kiki Tesselaar, PhD,[3] Peter van Kerkhof, PhD,[1] Jan Loeffen, MD, PhD,[2] Dimitris Grivas,[1] Eric Hennekam, MSc,[4] Jaap Jan Boelens, MD, PhD,[5] Peter M. Hoogerbrugge, MD, PhD,[2] Peter van der Sluijs, PhD,[1]* Marielle E. van Gijn, PhD,[4] and Lisette van de Corput, PhD[3]

Background. *UNC13D,* encoding the protein munc13-4, is essential in intracellular trafficking and exocytosis of lytic granules. Mutations in this gene are associated with familial hemophagocytic lymphohistiocytosis type 3 (FHL3), a genetically heterogeneous, rare autosomal recessive immune disorder. How mutations affect function of munc13-4 is poorly understood. Since 2006 we genetically identified seven FHL patients with mutations in *UNC13D*. ***Procedures.*** Here, we report for the first time a c.2695C>T (p.Arg899X) mutation in exon 28 of *UNC13D* in three young unrelated Dutch patients. The mutation causes a premature stop codon and encodes munc13-4(1–899), which lacks the C-terminal C2 domain. Genealogical research and haplotyping of the patient families demonstrated that a single ancestral founder introduced the mutation in the Netherlands. We then characterized the mutant protein phenotypically in cell biological and immunological assays. ***Results.*** Munc13-4(1–899) was correctly targeted to CD63-positive secretory lysosomes, although its stability was reduced and dynamic turnover on the granule membrane became uncoupled from receptor signaling. In accord, and in contrast to wild-type munc13-4, ectopically expressed mutant failed to rescue degranulation in cells with silenced endogenous munc13-4. ***Conclusions.*** The functional and clinical data showed that this novel Dutch founder mutation leads to severe early onset of FHL3 due to misfolding and degradation of munc13-4(1–899).
Pediatr Blood Cancer 2012;58:598–605.

Key words: C2B domain; degranulation; HLH; misfolding; munc13-4

INTRODUCTION

Hemophagocytic lymphohistiocytosis (HLH) is a collection of severe immune disorders of inherited and acquired forms. HLH is characterized by uncontrolled proliferation of activated lymphocytes and histiocytes that invade healthy organs such as liver, spleen, and brain. The disease is fatal unless treated [1]. Familial hemophagocytic lymphohistiocytosis (FHL) represents a heterogeneous autosomal recessive form of HLH that is caused by mutations in the genes encoding perforin (*PRF1*), munc13-4 (*UNC13D*), syntaxin 11 (*STX11*), or munc18-2 (*STXBP2*) (reviewed in Ref. 2). Mutations in these genes cause impaired lymphocyte-mediated cytotoxicity and defective triggering of apoptosis.

Patients with Chediak–Higashi syndrome or Hermansky Pudlak syndrome type 2 may also present with hemophagocytosis due to mutations in *LYST* and *AP3B1* (reviewed in Ref. 2). The identification of genes associated with HLH greatly contributed to our understanding of the pathophysiology of the disease and gave critical new insight in molecular mechanisms regulating the lytic granule pathway. It also led to the paradigm that efficient removal of target cells has an important role in homeostasis of lymphocytes, since genetic lesions affecting cytotoxicity cause uncontrolled expansion of cytotoxic lymphocytes and life-threatening HLH [1,2].

Perforin, the protein associated with FHL2 is required for the delivery of granzymes from the lytic granules into target cells [3]. Many of the *PRF1* missense mutants have been functionally characterized through expression studies in heterologous systems, of which particularly the RBL-2H3 rat basophil leukemia cell line proved to be very useful [4–7].

In contrast to *PRF1*, the other genes mutated in FHL encode members of conserved protein families that regulate fusion of granules and release of lytic content [8,9]. Munc13-4 controls fusion of lytic granules with the plasma membrane [10]. The mechanistic details, however, are far from being understood and we know little about the consequences of disease mutations on munc13-4 protein function.

We identified seven Dutch patients with mutations in UNC13D, three of which harbored a new c.2695C>T (p.Arg899X) mutation, causing a stop codon in exon 28. The mutation originates from a common founder and resulted in severe early-onset of HLH in three patients. The nonsense mutation in exon 28 encodes a truncated protein, that is, properly targeted to granules, but faster degraded. The mutation affects munc13-4 exchange kinetics on granules and cannot rescue degranulation in the absence of endogenous munc13-4, showing that it is functionally inactive.

PATIENTS AND METHODS

Patients and Controls

All patients fulfilled the criteria of HLH (see Table I) and written informed consent by the families was given. Peripheral blood mononuclear cells (PBMC) from healthy donors were used as controls.

[1]Department of Cell Biology, UMC Utrecht, Utrecht, The Netherlands; [2]Department of Pediatrics Hemato-Oncology, Radboud University Nijmegen Medical Center, Nijmegen, The Netherlands; [3]Department of Immunology, UMC Utrecht, Utrecht, The Netherlands; [4]Department of Medical Genetics, UMC Utrecht, Utrecht, The Netherlands; [5]Department of Pediatric Immunology, UMC Utrecht, Utrecht, The Netherlands

Grant sponsor: Dutch Cancer Society.

Conflict of interest: Nothing to declare.

*Correspondence to: Peter van der Sluijs, PhD, Department of Cell Biology, University Medical Center Utrecht, Heidelberglaan 100, 3584 CX Utrecht, The Netherlands.
E-mail: p.vandersluijs@umcutrecht.nl

Received 11 February 2011; Accepted 25 May 2011

DOI 10.1002/pbc.23253
Published online 13 July 2011 in Wiley Online Library (wileyonlinelibrary.com).

TABLE I. Mutations Found in Dutch FHL3 Patients

Patient	Allele 1	Exon	Allele 2	Exon
1	c.2695C>T	28	c.2695C>T	28
2	c.2695C>T	28	c.2695C>T	28
3	c.2695C>T	28	c.2988_3013del26	31
4	c.247C>T	3	c.754-2A>G	Intron 9
5	c.247C>T	3	c.2672T>C	28
6	c.551G>A	6	c.1148_1149insGG	13
7	c.1055+1G>A	Intron 12	c.1055+1G>A	Intron 12

Mutation and Haplotype Analysis

Granulocytes were isolated from peripheral blood using Ficoll gradient centrifugation and genomic DNA was isolated with the Autopure kit (Qiagen, Venlo, The Netherlands). Exon-specific M13-tagged primers were used to amplify all coding exons including flanking regions of the *UNC13D* (NCBI reference sequence (RefSeq): NM_199242.2), *PRF1* (NCBI RefSeq: NM_005041.4), or *STX11* (NCBI RefSeq: NM_003764.3) genes. Primer sequences are available upon request. Each exon was amplified in duplicate and sequenced on both strands using BigDye Terminator v1.1 (Applied Biosystems, Nieuwekerk a/d Ijssel, The Netherlands) cycle sequencing. Haplotype analysis was performed using the STS markers D17S1862, D17S1864, D17S1301, D17S1817, D17S937, and D17S801 surrounding *UNC13D*.

Antibodies

The rabbit antibody against munc13-4 (aa 1–262) was provided by Hisanori Horiuchi [11]. An antibody against the C-terminus of munc13-4 was raised by immunizing rabbits with GST-munc13-4(aa 904–1021). The rabbit antibody against GFP was from BD Biosciences, Breda, The Netherlands. Mouse monoclonal antibodies were obtained from the indicated sources: anti XPRESS (Invitrogen, Breda, The Netherlands), FITC-anti-CD107a, and rat CD63 (BD Biosciences). Mouse monoclonal IgE antibody (clone SPE-7) against DNP was from Sigma (Zwijndrecht, The Netherlands) and conjugated secondary antibodies were from Jackson ImmunoResearch (Uden, The Netherlands) and Rockland Immunochemicals (Heerhugowaard, The Netherlands).

PCR Amplification and cDNA Constructs

mRNA was isolated from spleen and PBMC, reverse transcribed and cDNA of munc13-4 nt 1–250 was amplified using primers 5′-ATGGCGACACTCCTCTCCC-3′ and 5′-GGAAGGCCTCCTGCAGGT-3′. β_2 microglobulin served as control and was amplified with primers 5′-GGCTATCCAGCGTACTCCAAA-3′ and 5′-CGGCAGGCATACTCATCTTTTT-3′. The patient mutant cDNA construct munc13-4(1–899) was generated by PCR and subcloned in pcDNA3.1HisB, peYFP-C2, peCFP-C2, and peGFP-C2.

Cell Lines, Transfection, and Lentiviral Transduction

PBMC and granulocytes were isolated from heparinized peripheral blood by Ficoll Paque centrifugation. The RBL-2H3 mast cell line was grown as described [12]. The following siRNAs targeting rat munc13-4 were purchased from Applied Biosystems: GGAACAAGAUUUUUCACAAtt (siRNA#1) and GUUGAAUGGUUUCACCUGAtt (siRNA#2). RBL-2H3 cells were transfected with 200 pmol using Amaxa nucleofection, kit T, program X-001 according to the manufacturers' instructions. HEK293T cells were grown and transfected as before [12]. Fluorescent protein-tagged munc13-4 cDNAs were inserted in pLNT-SFFV-WPRE-Gateway and used for virus production in HEK293T cells using helper plasmids psPAX2 and pMD2.G [12]. RBL-2H3 cells were transduced with lentiviruses and cells expressing YFP-tagged munc13-4 constructs were isolated by flow cytometry. All synthetic DNA was verified by dye termination sequencing of both strands.

Degranulation and Cytotoxicity Assays

Perforin expression in PBMC was determined ex vivo in $CD3^-CD16^+CD56^{dim}$ NK cells and different $CD8^+$ T cell subsets (defined by CD28 and CD45RA expression, that is, naive $CD28^+CD45RA^+$, memory $CD28^+$ $CD45RA^-$, memory effector $CD28^-CD45RA^-$ and effector $CD28^-CD45RA^+$), by staining with fluorescently labeled monoclonal antibodies (Becton Dickinson, Breda, The Netherlands). Degranulation was assayed by cell surface appearance of CD107a on NK cells ($CD3^-CD16^+CD56^+$) [13]. Briefly, PBMC were incubated for 4 hours with K562 cells at a 1:1 ratio in the presence of FITC-labeled CD107a. Cells were harvested and CD107a expression was measured on the $CD3^-CD16^{++}CD56^{dim}$ population by flow cytometry and analyzed with CellQuest Pro software. Data are presented as increase during the 4 hours (t_4–t_0) period. Degranulation in RBL-2H3 cells was assayed as release of the secretory lysosome content marker β-hexosaminidase as described [14].

Protein Assays

Frozen spleen biopsies were crushed and protein was extracted in 25 mM Tris–HCl, pH 7.6, 150 mM NaCl, and protease inhibitors (Roche, Almere, The Netherlands). Samples were sonicated for 30 seconds, and lysed in PBS, 1% TX-100, 0.1% SDS. Stability of munc13-4(1–899) was investigated by expressing His6-tagged constructs in HEK293T cells. After 18 hours, cells were incubated at 37°C in the presence of 0.35 mM cycloheximide or 20 μM MG132. Cells were lysed after different periods of time in 1% TX-100, 50 mM Tris–HCl, pH 7.6 and cleared by centrifugation during 5 minutes at 14,000 rpm and 4°C. Pellets were extracted with reducing Laemmli buffer containing 2% SDS. For some experiments, cells were lysed in 50 mM

Tris–HCl, pH 7.6, 1% octylglucoside. Lysates were resolved on 7.5% SDS–PAA gels, subjected to Western blot with antibody against XPRESS epitope. Quantitation was with an Odyssey infra-red imager (Li-Cor, Leusden, The Netherlands). Human tissue and PBMC samples were analyzed by Western blot with rabbit antibodies against munc13-4.

Fluorescence Microscopy and Quantitative Image Analysis

Transfected RBL-2H3 cells were processed for immunofluorescence microscopy as described [12]. Coverslips were examined with a Zeiss LSM 510 confocal microscope using a 63× oil objective. Image sets to be compared were acquired during the same session and using the same acquisition settings. Image analysis was performed with the Volocity software suite (version 5.2 Improvision). For colocalization of munc13-4 positive structures, we obtained z-stacks of at least 10 slices with optimal thickness for the pinhole. Thresholds for intensity were manually set on control samples and 3D volumes were obtained. To find overlap between structures identified in two independent channels, the 3D volumes were analyzed for overlap. For colocalization statistics the total overlapping volume was compared to the total amount of volume per channel.

Fluorescence Recovery after Photobleaching (FRAP)

FRAP experiments were performed on transfected RBL-2H3 cells in a climate-controlled chamber with 5% CO_2 at 37°C as described [12]. Briefly, cells were kept in 0.75 ml DMEM, 1% FCS without phenol red. After equilibration cells received 0.25 ml prewarmed medium containing 4 μM ionomycin, 400 nM PMA, and 10 ng/μl of the styryl dye FM4-64 (Invitrogen) to induce a fast and homogeneous activation. Imaging was started 90 seconds after the addition of the drugs, when most cells showed first signs of degranulation. Activated cells were identified by the presence of FM4-64 which entered secretory lysosomes after fusion at the plasma membrane [12]. Imaging was performed on a Zeiss 510 LSM with ZEN (Carl Zeiss, Sliedrecht, The Netherlands) software and FRAP analysis was then performed as we described before [12].

Statistical Analysis

Statistical analysis of data was performed on the average of three independent experiments. To evaluate the statistical significance we used single factor ANOVA and *t*-tests for individual significance between two samples. *P* values below 0.05 were considered statistically significant.

RESULTS AND DISCUSSION

New UNC13D Mutation in Dutch Patients

Since 2006 we genetically identified seven FHL3 patients in our University Medical Center Utrecht (Table I). Six mutations were new and two were described before. Three very young Dutch children with prolonged fever and diagnosed for HLH (Table II) showed the same new c.2695C>T (p.Arg899X) mutation in exon 28 of *UNC13D*. This mutation was not present in 100 healthy donors (200 alleles). Genealogical research, where two patients could be traced to a common link (Fig. 1A), and haplotype analysis demonstrated that a single ancestral founder introduced the mutation in the Netherlands. PBMC from two patients could be analyzed for degranulation of NK cells. Cell surface appearance of CD107a in $CD3^{-}CD16^{++}CD56^{dim}$ patient cells was markedly reduced, compared to control PBMC (Fig. 1B). The c.2695C>T (p.Arg899X) mutation introduces a premature stop codon which generates munc13-4(1–899) and lacks the C-terminal C2B domain (Fig. 2A).

TABLE II. Characteristics of the Three Dutch Patients With HLH at Admission

	Case 1	Case 2	Case 3
Age at onset (weeks)	6	8	12
Gender	Boy	Girl	Girl
Consanguinity	No	No	No
Fever (days)	7	10	19
Cytopenia in >2 cell types[a]	Yes, P	Yes, A+T	Yes, A+T
(Hepato)Splenomegaly	Yes	Yes	Yes[b]
Fibrinogen (mg/L)	790	1,500	1,310
Triglycerides (mmol/L)	2.93	5.19	6.5
Ferritin (mg/L)	4,678	2,353	5,842
NK cell activity	Decreased	Detectable	Not determined
Perforin expression[c]	Normal	Normal	Normal
Soluble CD25 (U/ml)	>7,000	>7,200	30.565
Hemophagocytosis BM	No	No	Yes
CNS involvement	Yes	Yes	Probably
Mutation in UNC13D	c.2695C>T[d]	c.2695C>T[e]	c.2695C>T[e]
HLH-2004 protocol	Yes	Yes	Yes
HCST	Yes	No	No
Outcome	Deceased (6 months)	Deceased (6 months)	Deceased (5 months)

[a]P, A, T denote pancytopenia, anemia and thrombocytopenia, respectively; [b]Hepatosplenomegaly became manifest a few days after presentation; [c]Assayed in NK and CD8+ T cells; [d]Compound heterozygosity for c.2695C>T in exon 28 and c.2988_3013del26 in exon 31; [e]Homozygous.

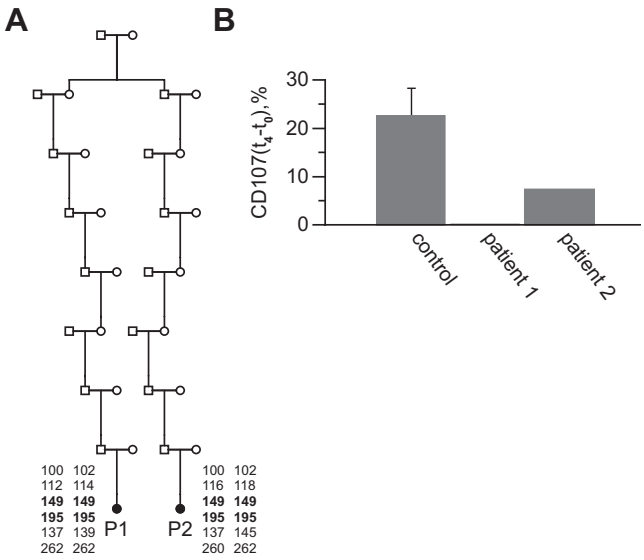

Fig. 1. Characterization of new FHL3 patients. Pedigree analysis of Dutch FHL3 patients 1 and 2 showing that the patients can be traced back to a common ancestor and shared the same haplotype. Both were homozygous for all SNPs in UNC13D and shared STS markers at both sides of the gene D17S1301 (149) and D17S1819 (195). The other markers did not segregate with the mutation. All mutation carriers, including patient 3 (not shown) had the 149–195 haplotype (**A**). Increase (during 4 hours) in surface expression of CD107a on $CD3^{-}CD16^{+}$ $CD56^{dim}$ NK cells stimulated with K562 cells in the presence of FITC-labeled anti-CD107a, the control group consisted of 32 individuals (**B**).

Munc13-4(1–899) Expression

To evaluate munc13-4(1–899) expression, we analyzed patient samples by Western blot with antibodies against the N- or C-terminus of munc13-4. The first one detects full length wild-type munc13-4 and the truncation mutant, while the C-terminal antibody will not detect the truncation mutant (Fig. 2A). Because the condition of the patients did not allow us to obtain additional PBMCs for assaying protein, we employed a frozen spleen biopsy (patient 2) for this analysis. Both antibodies recognized full length protein in PBMC extracts of the parents (from patient 2) and in the healthy control spleen sample (Fig. 2B). Using standard protein extraction, the truncated protein was not detected with the antibody against the N-terminus both in patient and heterozygous parent samples (Fig. 2B). We next investigated if mRNA encoding munc13-4(1–899) could be degraded via non-sense-mediated mRNA decay [15]. We detected however mRNA for munc13-4(1–899) by RT-PCR in spleen biopsies of patient 2 (Fig. 2C), suggesting that the absence of munc13-4(1–899) protein in TX-100 lysates is caused by misfolded or degradation.

Absence of the C2B Domain Enhanced Aggregation and Degradation

To investigate stability of mutant munc13-4, we transfected His-tagged expression constructs in HEK293T cells. Cells were incubated with the protein synthesis inhibitor cycloheximide and lysed after different periods of time in TX-100 buffer. Munc13-4 decreased gradually during the 8 hours chase (Fig. 3A), both in the cleared lysate and TX-100 insoluble fraction. About 50% was still present after 8 hours, showing that it is a relatively stable protein, while over 80% of munc13-4(1–899) had disappeared.

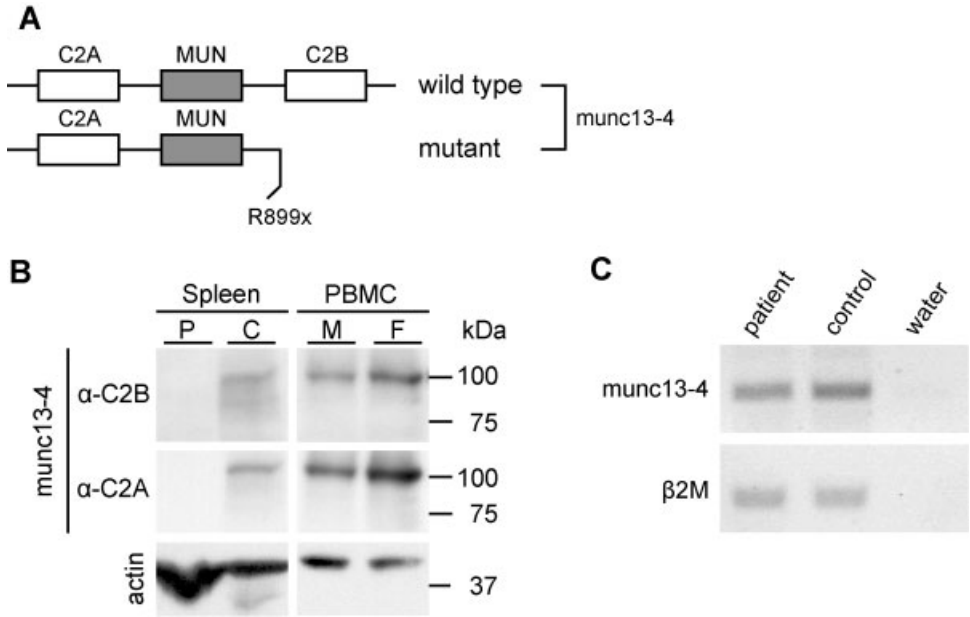

Fig. 2. Expression of munc13-4(1–899) in patient samples. Domain representation of munc13-4 (**A**), Western blot of munc13-4 in spleen samples of patient 2 (P) and control (C), and in PBMC of patient's mother (M) and father (F) heterozygous for the c.2695C>T mutation. Note the absence of a truncated form that should be detectable with the antibody against the C2A domain but not with the C-terminal C2B antibody (**B**), RT-PCR of munc13-4 mRNA isolated from patient 2 and control spleen samples using oligo's annealing to exons 1 and 3 amplifying the first 250 nucleotides of the coding sequence. β_2 microglobulin (β2M) was used as control (**C**).

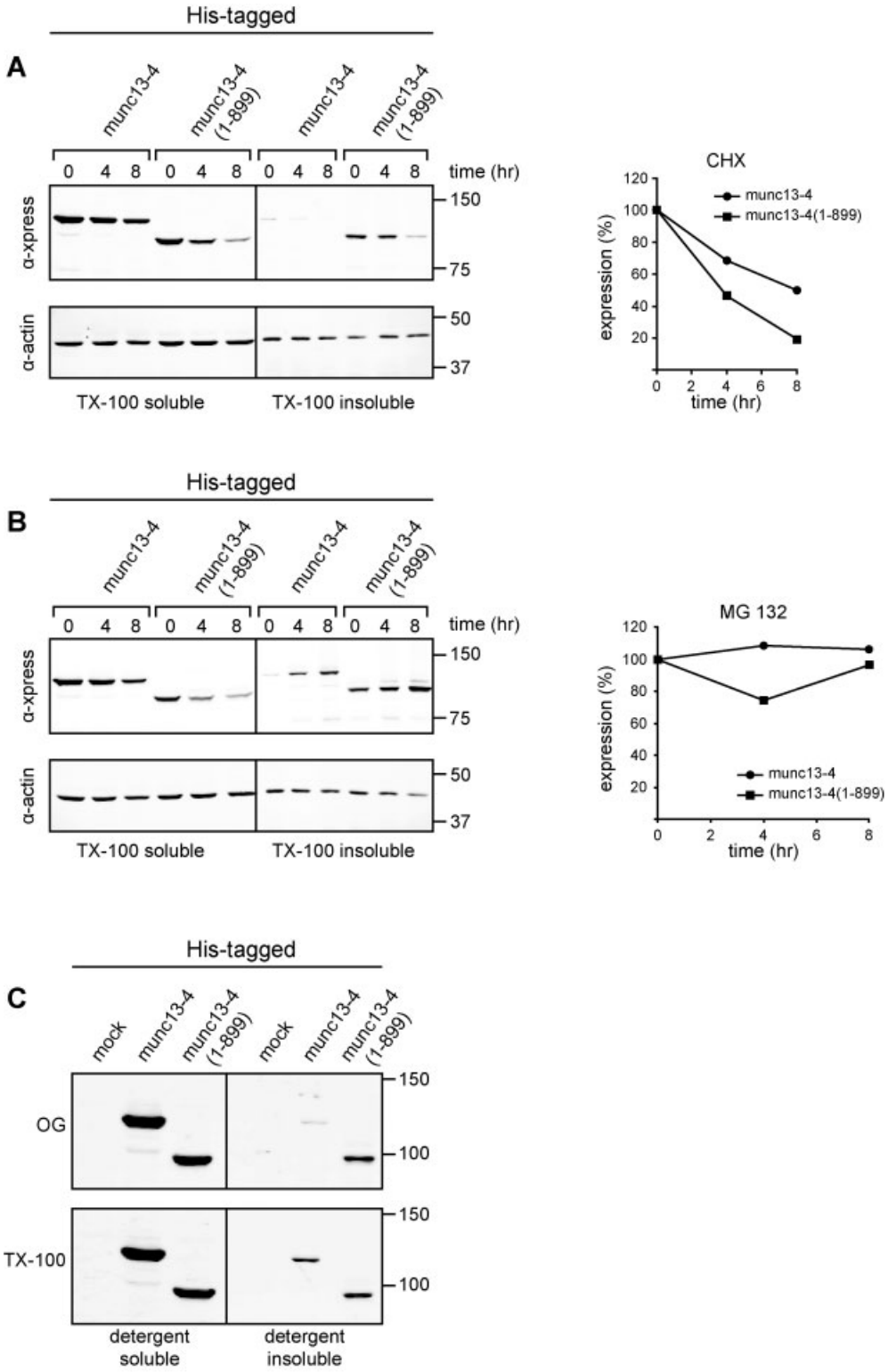

Fig. 3. Lack of the C2B domain caused aggregation of munc13-4(1–899) and degradation. Expression of His_6munc13-4 and His_6munc13-4(1–899) in HEK293T cells in which protein synthesis was inhibited with 0.35 mM cycloheximide (**A**) or proteasomal degradation was inhibited with 20 μM MG132 (**B**). Quantitations in A and B represent the total amount of His-tagged munc13-4 or munc13-4(1–899) proteins present in the TX-100 soluble and insoluble fractions. Cell extracts were prepared in 1% TX-100 or 1% octylglucoside (OG) lysis buffer, and proteins in cleared lysate and nuclear pellet were analyzed by Western blot with Xpress monoclonal antibody and a monoclonal antibody against actin. The same amount of munc13-4(1–899) was solubilized under both conditions showing that the mutant does not partition to lipid rafts (**C**).

During this period of time, the amount of aggregated munc13-4(1–899) in the TX-100 insoluble fraction was three- to fivefold higher than for munc13-4 (Fig. 3A). The increased turnover and aggregation of munc13-4(1–899) suggested that the mutant might be misfolded and degraded in the proteasome. In agreement with this, the proteasome inhibitor MG132 increased the fraction of munc13-4(1–899) and wild-type munc13-4 that was insoluble in TX-100 (Fig. 3B, right part of the Western blot) with a parallel decrease in the TX-100 soluble fraction (Fig. 3B, left part of the Western blot). The sum of munc13-4(1–899) present in the combined TX-100 soluble and TX-100 insoluble fractions was relatively constant, as was seen with wild-type munc13-4 (Fig. 3B, graph). These results show that enhanced degradation of the munc13-4(1–899) mutant protein in Figure 3A, was to a large extent prevented by the addition of MG132. TX-100 insolubility of munc13-4(1–899) was not caused by partitioning in a detergent resistant membrane domain with raft properties [16] because insoluble munc13-4(1–899) amounted to 13% in octylglucoside- and 14% in TX-100 lysates (Fig. 3C). Collectively the biochemical characterization showed that mutant munc13-4(1–899) was normally synthesized but attains a conformation which is distinct from wild-type munc13-4. The loss of the C2B domain caused misfolding that enhanced proteasomal degradation, and impaired solubilization in non-denaturing lysis buffers. This also provides an explanation for the absence of munc13-4(1–899) in spleen lysates prepared from the patient.

Munc13-4(1–899) Fails to Rescue Degranulation in a Knock-Down Model

We next characterized the novel FHL3 mutation functionally using a novel complementation assay in the RBL-2H3 cell model. Secretory lysosome release in this tumor mast cell line critically relies on munc13-4 [12]. We introduced siRNA resistant YFP-tagged human munc13-4 variants by lentiviral transduction, and then silenced endogenous rat munc13-4 with siRNAs that yielded >90% knock down (Fig. 4A). Degranulation of cells with knock-in munc13-4 constructs was measured as IgE/DNP-HSA stimulated release of β-hexosaminidase. Silencing of endogenous munc13-4 reduced β-hexosaminidase release fivefold compared to cells that were transfected with a scrambled control oligo (Fig. 4B). Cells expressing munc13-4(1–899), failed to rescue the loss of β-hexosaminidase secretion after knock-down of endogenous munc13-4, while wild-type munc13-4 complemented to near control levels (Fig. 4B). Expression of munc13-4(1–899) in the background of endogenous protein did not affect degranulation significantly, showing that the mutant does not act as a dominant negative, explaining why heterozygote carriers are not affected (Fig. 4C).

Munc13-4(1–899) Exchange on Granules Is Impaired During Degranulation

We recently showed that cytoplasmic munc13-4 translocates to, and dissociates off granule membrane as part of a functional cycle [12]. Using confocal fluorescence microscopy we determined that munc13-4(1–899) localized extensively to CD63-containing secretory lysosomes (Fig. 5B) like wild-type munc13-4 (Fig. 5A), with Manders coefficients for colocalization [17] of 0.93 and 0.96, respectively. In agreement with the high degree

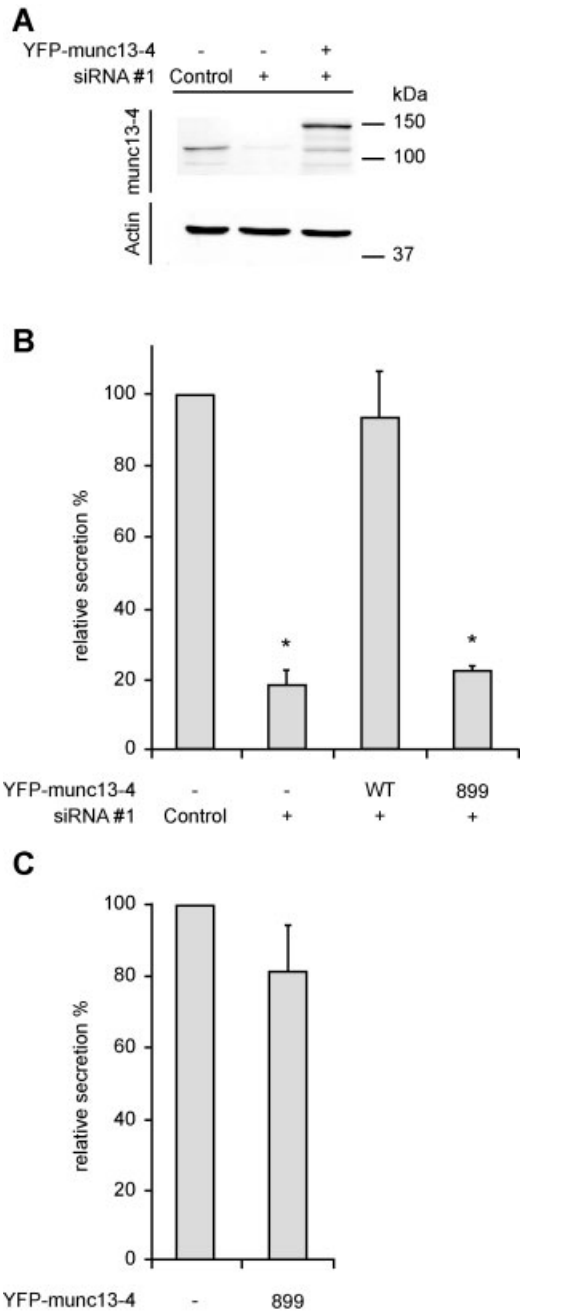

Fig. 4. Munc13-4(1–899) does not rescue loss of secretion. Western blot of lysates from RBL-2H3 cells with 200 nM (final concentration) of siRNA#1, or control scrambled siRNA. After 2 days munc13-4 expression was reduced to 10% by siRNA#1 (**A**). Complementation analysis of IgE/DNP-HSA triggered β-hexosaminidase secretion in RBL-2H3 cells with silenced endogenous munc13-4 and knock-in of YFP-tagged siRNA resistent munc13-4 constructs. Data are means ± SE of three experiments, asterisks denote $P < 0.01$ (**B**). Secretion of β-hexosaminidase in RBL-2H3 expressing YFP-munc13-4(1–899), or mock-transfectant with normal levels of endogenous rat munc13-4 (**C**).

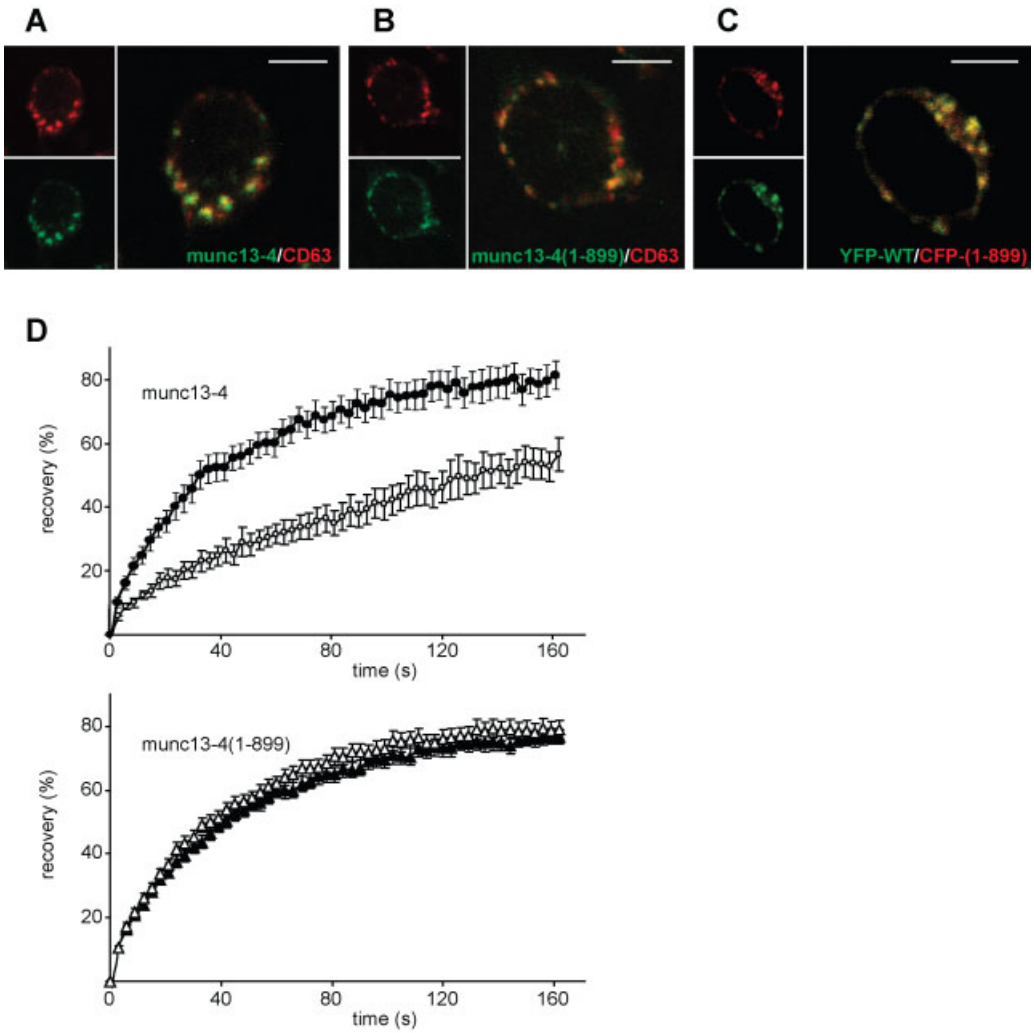

Fig. 5. Munc13-4(1–899) exchange on granules is impaired in activated cells. Colocalization of YFP-munc13-4 (**A**) and YFP-munc13-4(1–899) (**B**) with CD63 (red) in RBL-2H3 cells. Colocalization of YFP-munc13-4 (green) and CFP-munc13-4(1–899) (red) in RBL-2H3 cells (**C**). FRAP analysis of resting (closed symbols) and activated (open symbols) RBL-2H3 cells expressing YFP-munc13-4(1–899) (triangles) and YFP-munc13-4 (circles) (**D**). Bar denotes 5 μm.

of colocalization with CD63, we detected CFP-munc13-4(1–899) and wild-type YFP-munc13-4 largely on the same structures (Fig. 5C). This property allowed us to directly compare their turnover on the granule by FRAP. YFP emission of single discrete granules seen in Figure 5A was bleached and recovery of fluorescence from the cytoplasm was measured every 2 seconds by automated time-lapse confocal microscopy. Re-appearance of YFP fluorescence was not due to ongoing membrane trafficking, because fluorescence of a granule content marker did not recover. Munc13-4 granule fluorescence recovered to 81.0 ± 4.9% with a half time of 43.7 ± 3.7 seconds (Fig. 5D). In degranulating cells, FRAP parameters were changed to 56.5 ± 7.9% and 72.0 ± 9.9 seconds, respectively. Since munc13 proteins are thought to act in trans priming of cognate SNARE complexes [18], the reduced mobility and the nearly doubled half time likely reflect the engagement of munc13-4 in protein–protein interactions during granule priming, or anchoring to the cytoskeleton. Interestingly, mobility of neuronal munc13-1 is subject to modulation by synaptic activity [19]. YFP–munc13-4(1–899) fluorescence recovered to 76.8 ± 7.6% with a halftime of 42.0 ± 3.6 seconds, representing kinetics very similar to that of wild-type munc13-4. Importantly, FRAP parameters of YFP–munc13-4(1–899) were not affected (recovery: 79.4 ± 1.7% and halftime 49 ± 4.5 seconds), showing that degranulation was uncoupled from receptor signaling for the mutant. The absence of characteristic mobility changes in a patient mutant that lacks the C-terminal C2 domain is in accordance with the degranulation defect of the FHL3 mutation and provides a molecular explanation for impaired function of munc13-4. C2 domains are multifacetted interaction platforms that engage in protein–protein interactions, Ca^{2+}, and lipid binding [20]. In agreement with this, the C-terminal C2 domain of munc13-4 binds phospholipids in vitro [21]. Future studies will therefore be directed toward identifying the signaling pathways regulating munc13-4 and its connection with the SNARE complex involved in granule fusion.

In summary, we describe the new c.2695C>T (p.Arg899X) mutation in exon 28 of *UNC13D*, which introduces a stop codon immediately upstream of the C-terminal C2B domain. Misfolding of the mutant correlates with altered exchange kinetics on granules, and failure to rescue degranulation. The functional and clinical data provide a molecular explanation for the deficiency, which resulted in severe early-onset of FHL3.

ACKNOWLEDGMENT

This work was supported by a grant of the Dutch Cancer Society (to PvdS). We thank Chantal Cornelissen for haplotyping, Rene Scriwanek for preparation of figures, and colleagues for reagents.

REFERENCES

1. Fischer A, Latour S, de Saint Basile G. Genetic defects affecting lymphocyte cytotoxicity. Curr Opin Immunol 2007;19:348–353.
2. Schmid JP, Cote M, Menager MM, et al. Inherited defects in lymphocyte cytotoxic activity. Immunol Rev 2010;235:10–23.
3. Pipkin ME, Lieberman J. Delivering the kiss of death: Progress on understanding how perforin works. Curr Opin Immunol 2007;19:301–308.
4. Bossi G, Griffiths G. Degranulation plays an essential part in regulating cell surface expression of Fas ligand in T cells and natural killer cells. Nat Med 1999;5:90–96.
5. Voskoboinik I, Smyth MJ, Trapani JA. Perforin mediated target cell death and immune homeostasis. Nat Rev Immunol 2006;6:940–951.
6. Moreno RU, Gil J, Sainz CR, et al. Functional assessment of perforin C2 domain mutations illustrates the critical role for calcium-dependent lipid binding in perforin cytotoxic function. Blood 2009;113: 338–346.
7. Risma KA, Frayer RW, Filipovich AH, et al. Aberrant maturation of mutant perforin underlies the clinical diversity of hemophagocytic lymphohistiocytosis. J Clin Invest 2006;116:182–192.
8. Stinchcombe JC, Griffiths GM. Secretory mechanisms in cell-mediated cytotoxicity. Annu Rev Cell Biol Dev Biol 2007;23:495–517.
9. Sudhof TC, Rothman JE. Membrane fusion: Grappling with SNARE and SM proteins. Science 2009; 233:474–477.
10. Feldmann J, Callebaut I, Raposo G, et al. Munc 13-4 is essential for cytolytic granules fusion and is mutated in a form of Familial Hemophagocytic Lymphohistiocytosis (FHL3). Cell 2003;115:461–473.
11. Shirakawa R, Higashi T, Tabuchi A, et al. Munc 13-4 is a GTP-rab27 binding protein regulating dense core granule secretion in platelets. J Biol Chem 2004;279:10730–10737.
12. Elstak E, de Jong A, van der Sluijs P. A platform for complementation and characterization of familial haemophagocytic lymphohistiocytosis 3 mutations. J Immunol Methods 2011;358:58–66.
13. Alter G, Malenfant JM, Altfeld M. CD107a as a marker for the identification of NK cell activity. J Immunol Methods 2004;294:15–22.
14. Neeft M, Wieffer M, de Jong AS, et al. Munc 13-4 is and effector of rab27a and controls secretion of lysosomes in haematopoietic cells. Mol Biol Cell 2005;16:731–741.
15. Rebbapraganda I, Lykke-Andersen J. Execution of nonsense-mediated mRNA decay: What defines a substrate? Curr Opin Cell Biol 2009;21:394–402.
16. Brown DA, London E. Functions of lipid rafts in biological membranes. Annu Rev Cell Dev Biol 1998;14:111–136.
17. Bolte S, Cordelieres FP. A guided tour into subcellular localization analysis in light microscopy. J Microsc 2006;224:213–232.
18. Guan R, Dai H, Rizo J. Binding of the Munc 13-1 MUN domain to membrane-anchored SNARE complexes. Biochemistry 2008;147:1474–1481.
19. Kalla S, Stern M, Basu J, et al. Molecular dynamics of a presynaptic active zone protein studied in munc 13-4 enhanced YFP knock in mutant mice. J Neurosci 2006;26:13054–13066.
20. Shao X, Li C, Fernandez I, et al. Synaptotagmin-syntaxin interaction: The C2 domain as a Ca^{2+} dependent electrostatic switch. Neuron 1997;18:133–142.
21. Pivot-Pajot C, Varoqueaux F, de Saint Basile G, et al. Munc 13-4 regulates secretion in human neutrophils. J Immunol 2008;180:6786–6797.